Tuijin Jishu/Journal of Propulsion Technology
ISSN: 1001-4055
Vol. 44 No. 4 (2023)

One Dimensional (1D) Column Buckling Factor Analysis of Al-2024 Alloy Panel

[1]Syed Kashif Hussain, [2]Mir Safiulla
[1,2]Ghousia College of Engineering, Ramanagaram, Visvesvaraya Technological University, Belagavi – 590018, Karnataka, INDIA

Abstract:-The failure mode of buckling in science is caused by mathematical instability. Material failures and structural variability, acknowledged as buckling, are two of the most common causes of the failure of mechanical components suddenly. Whenever a wall made of a larger material than either of the two other dimensions of the wall is put under axial compression, because of its size, its axial displacement will be much smaller than the size of its lateral deflection, which is a phenomenon known as buckling. In the present study, Al 2024 alloy panel, is used for buckling factor analysis and understanding the effect of boundary conditions based on Euler's formulae approach. The buckling factor was obtained for different boundary conditions by taking the length, width, and thickness panel. The theoretical buckling factor is calculated using the abovementioned formula for other boundary conditions. Then the panel analysis is done in Nastran-Patran software for different boundary conditions to compare results.

Keywords*: Buckling, Euler's formulae, Al2024 alloy, Boundary conditions.*

1. Introduction

Composite is a material made up of fibres or particles embedded in another material. A laminate is a versatile material made up of several layers of materials that give it the unique character that allows it to perform an exceptional function as a composite material [1]. In addition to their lack of a matrix, fabrics have a variety of fibre compositions that, when combined, give them a unique character that makes them stand out. Generally, reinforcement materials are capable of withstanding maximum loads while serving the desired properties at the same time [2]. There is, however, no clear discernment that can really be made of composite types from one another, even though they are typically distinguishable [3]. This can be accomplished by shifting the emphasis to the level of differentiation that is taking place, that is, microscopic or macro level, to facilitate definition. In the case of structural composites made from matrix-based reinforcing elements, the matrix serves two critical functions: securing the reinforcement phases together under an applied force and deforming so that the stresses are distributed evenly throughout the composite pattern [4]. There are two distinct levels of classification of composite materials that are commonly used in the classification process; the matrix constituents are usually considered at the first level, which are metal, ceramic and polymer matrix composites are the three main composite classifications, followed by particulate composite, fibre reinforced composites, and laminar composites are included in the classification of the second level for the kind of reinforcement [5]. As the name implies, reinforcements are fibrous, strong, nonwoven materials incorporated into matrix materials to make the physical characteristics better than earlier. As reinforcements, various materials are used, such as synthetic fibre, carbon, jute, graphite, glass, boron, CNTs, and ceramics such as SiC, B4C, TiC, Al2O3 etc [6-9]. The purpose of reinforcements is to increase the flexural as well as tensile strength of the structure, while the purpose of fillers is not specified [10]. The purpose of reinforcement is to strengthen the joint by creating a bond. Reinforcement is typically used to increase the strength of a resin system by improving its mechanical properties. Even though composite material's original strength comes from its fibres, the matrix also plays a significant role in giving the composite material strength since it holds the fibres in place and enables them to carry loads. Moreover, matrices also provide a bonding agent that binds and stabilizes composite materials at the

same time. There are two composite types, resin-rich and fibre-rich composites [11]. Resin-rich composites have more resin than fibres, whereas fibre-rich composites have a smaller amount than fibres. Resin-rich composites have a higher tendency to crack [12-13].

In contrast, resin-starved composites are less likely to be strong as fibres are arranged improperly, and the resin does not provide enough support leading to cracks occurring during processing. It is essential to emphasize the fibres' functions, such as holding the fibres together, providing protection from the environment, distributing loads within the fibres, improving the ability of composites to withstand fractures and impacts, avoiding crack propagation, and enhancing the composites' transverse properties [14]. The matrix should display the following properties: low coefficients of thermal expansion, low moisture absorption, high strength, good modulus, and good elongation. Examples of resins include vinyl ester, polyester, phenolic, epoxy, and polyester [15].

The present study aimed to examine the effect of stiffened plates in wing box structures on the buckling load, which is calculated using the finite strip method developed by Eduard Risks. During the flight, the top skin of the top surface of an aircraft is subjected to compressive forces resulting in bulging variability due to spars and braced panels of a wing to form thin-walled structures.

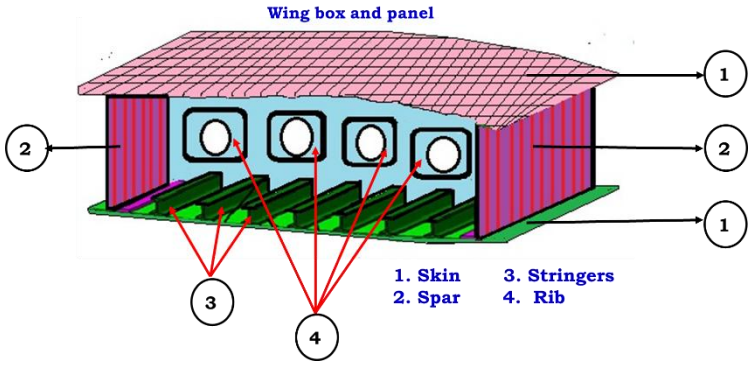

Figure 1: Wing box and panel

1.1. Overview of Wing Box

A heavier-than-air aircraft is primarily powered by its wings, with much of its lift produced by the wings. The wing structures are responsible for carrying a large amount of weight among the aircraft structures. Besides the aircraft's size and weight, many other factors affect how a wing is designed. These include the aircraft's size, weight, speed, and climbing rate. Under extreme stress conditions associated with combat maneuvers or the loading of the wing, the wing must be constructed to maintain its aerodynamic form [16]. At its most basic level, an aeroplane wing is a metal frame composed of ribs and spars, surrounded by a metal sheet covered by wings. The fundamental underlying sections of a wing are spars. Spars are the main component of the wings that carry all the load carried by the wings. There is a high degree of bending strength incorporated into the spars. The ribs give the wing part's model, which removes air load to the spars from the wing covering. The leading edge of the wing and the following edge both have ribs. Wings are complicated structures, so their evaluation might be challenging, so these structures must be simplified into structures that are easier to analyze. To make analysis easier, have accounted for the wing as a boxlike structure [17].

2. Material Details

Copper is the primary debasing element in the 2024 aluminum alloy followed by other elements as depicted in Table 1. It is utilized in a high strength to weight ratio and strong fatigue endurance applications are expected. It is only machinable to a fair extent and can only be welded via friction welding. Aluminum alloy 2024 has a density of 2.75 g/cm3, Young’s modulus and of 70 GPa and begins to melt at 570 °C. Al2024 has wide range of application due its advantages which includes formability, corrosion resistance, recyclability, strength, and lightness, which makes it an ideal material for a wide range of products and materials.

Table 1: Chemical composition of Al2024 alloy (Wt %)

Cu	Mg	Si	Zn	Others	Balance
4.5	1.4	0.44	0.23	0.05	Al (93.38)

2.1. Eulers Model Assumptions

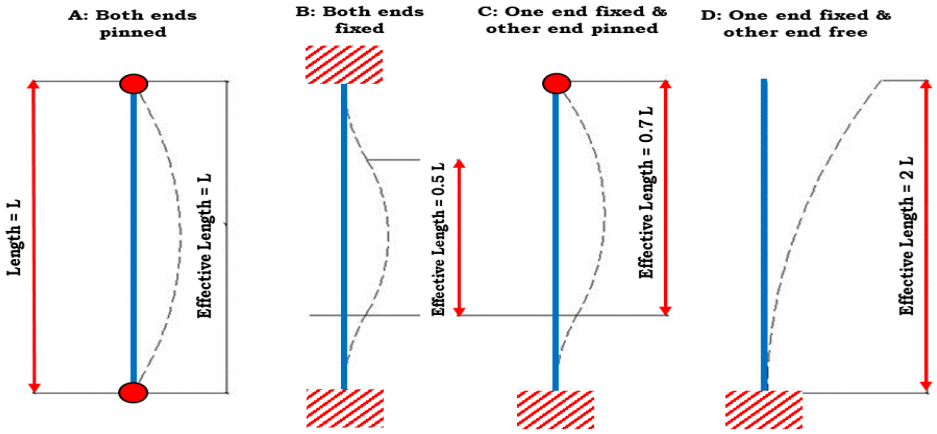

Figure 2: Effective length dimension for different boundary conditions

Euler's formula is derived based on several assumptions, including (i) The column's material is isotropic as well as homogeneous. (ii) The column is only under axial compressive load. (iii) There is no initial stress on the column. (iv) The column's weight is disregarded. (v) Assumed that the axial load is not eccentric at the start of the column. (vi) Fixed ends are rigid (no rotation deflection) and pin joints are frictionless (no moment constraint). (vii) Columns are uniformly cross-sectional throughout their length owing to their uniform cross-section. Only by buckling can the column fail. This's accurate if the column's compressive stress does not exceed its yield strength [18]. Effective length of column depends on boundary condition that is applied to the column.

3. Results and Discussions

1D analysis for understanding the effect of boundary conditions have been explained in the current section. Buckling factor obtained for different boundary conditions by taking the panel of length, width, thickness, and moment of inertia (IXX and IYY) considered as shown in Figure 3. Theoretical buckling factor is calculated by using the formula as explained above for different boundary conditions. Then the panel analysis is done in NASTRAN-PATRAN software for different boundary conditions to compare results. The calculations are done and tabulated as follow

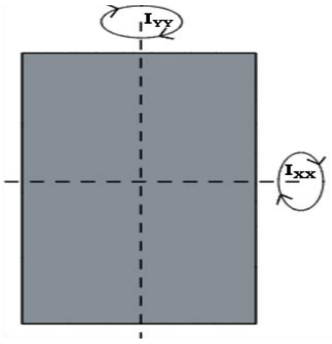

Figure 3: Depicting moment of inertia of Rectangular shape along X and Y axis

Figure 3 shows the moment of inertia of rectangular shape along X and Y axis, where Ixx=bd3/12 and Iyy=b3d/12. Here xx and yy imply path, being contemplated. In the field of structural engineering, it is widely accepted that the variable "b" denotes the width of a rectangle, aligned with the traditional horizontal x-axis. Likewise, the variable "d" denotes the vertical dimension of the rectangle, aligned with the usual y-axis.

3.1 Buckling Factor Calculations of Case 1 (b=d= 10 mm and L = 1000 mm)

The buckling factor (BF) is calculated by using the formula: BF = Critical load / Applied load. By considering the rectangular shape at applied load i.e., width of 10 mm, thickness of 10 mm and the length of panel 1000 mm.

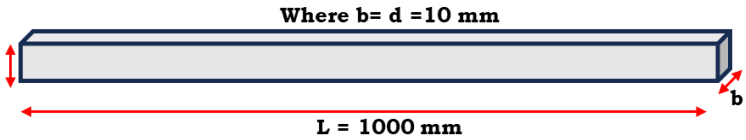

Figure 4: Rectangular shape of b=d= 10 mm and L= 1000 mm

The calculations are done based on the effective length dimension for different boundary conditions (Case A, B, C and D) as displayed in Figure 2, 3 and Eqn (i).

$$\mathbf{P_{cr} = \frac{\pi^2 EI}{L_e^2} \ldots\ldots (i)}$$

Where Pcr = Critical Load, E= Youngs Modulus, I = Moment of Inertia, Le = Effective Length

Table 1: Calculated values of different boundary conditions

S/No	Case	P_{cr}	E	I	L_e Conditions	BF
1	A	57.56	$70 *10^3$	833.33	$L_e = L$	0.5756
2	B	230.24			$L_e = 0.5L$	2.3024
3	C	115.12			$L_e = 0.7L$	1.1512
4	D	14.39			$L_e = 2L$	0.1439

Case A Calculations

$I = \frac{b*d^3}{12} = \frac{10*10^3}{12} = 833.33$; $P_{cr} = \frac{\pi^2*7000*833.33}{(1000)^2} = 57.56$; BF = 57.56 / 100 = 0.5756

Case B Calculations

$P_{cr} = \frac{\pi^2*7000*833.33}{(1000/2)^2} = 230.24$; BF = 230.24 / 100 = 2.3024

Case C Calculations

$P_{cr} = \frac{\pi^2*7000*833.33}{(0.7071*1000)^2} = 115.12$; BF = 115.12 / 100 = 1.1512

Case D Calculations

$P_{cr} = \frac{\pi^2*7000*833.33}{(2*1000)^2} = 14.39$; BF = 14.39 / 100 = 0.1439

3.1.1: Buckling Factor Using Nastran-Patran Analysis of Case 1

Theoretical buckling factor is calculated by as explained above for different boundary conditions. Then now the panel analysis is done in NASTRAN-PATRAN software for different boundary conditions to compare. And the results are tabulated as in table given below. %Error is also calculated for accuracy of calculations done in software and is calculated by using the formula below.

% Error = [(Theoretical BF – Analyzed BF) *100] / Theoretical BF……. (ii)

Table 2: Theoretical and analyzed values of case 1 for buckling factor at different boundary conditions

S/No	Case	L_e Conditions	BF (Theoretical)	BF (Analyzed)	%Error	Accuracy
1	A	$L_e = L$	0.5756	0.5756	0.0000	100.00000
2	B	$L_e = 0.5L$	2.3024	2.301	0.0608	99.93919
3	C	$L_e = 0.7L$	1.1512	1.1772	2.2585	97.74149
4	D	$L_e = 2L$	0.1439	0.1439	0.0000	100.00000

Case A: NASTRAN-PATRAN Analysis

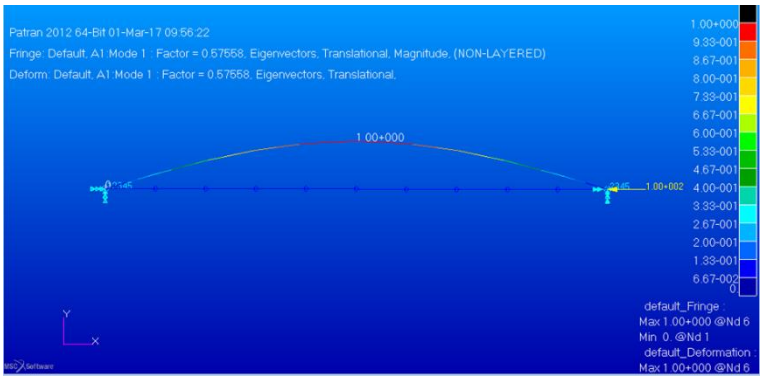

Figure 5(a): Buckling of column when both ends are hinged (Case 1)

Case B: NASTRAN-PATRAN Analysis

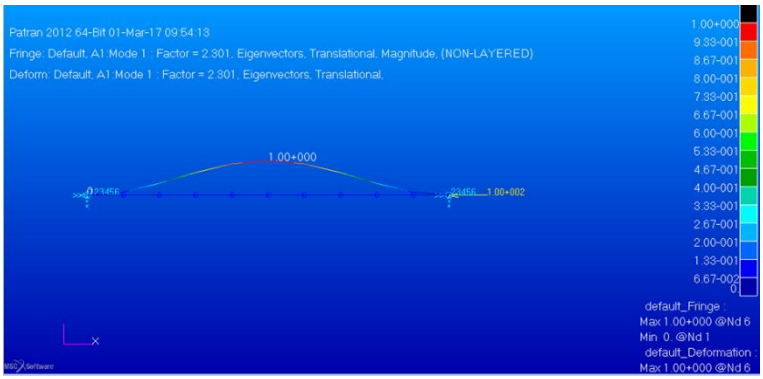

Figure 5(b): Buckling of Column when both ends are fixed (Case 1)

Case C: NASTRAN-PATRAN Analysis

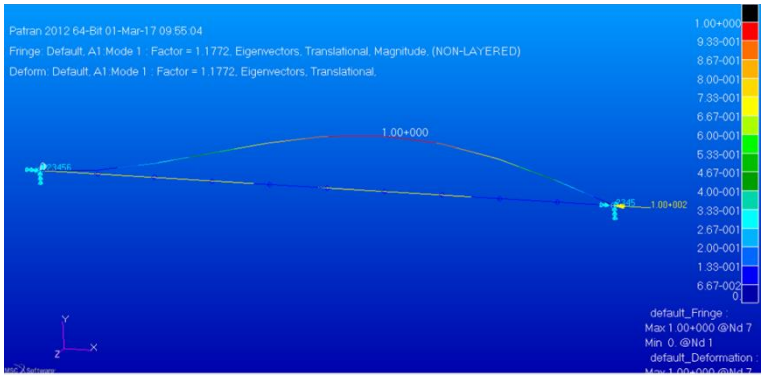

Figure 5(c): Buckling of Column when one end is fixed another is hinged (Case 1)

Case D: NASTRAN-PATRAN Analysis

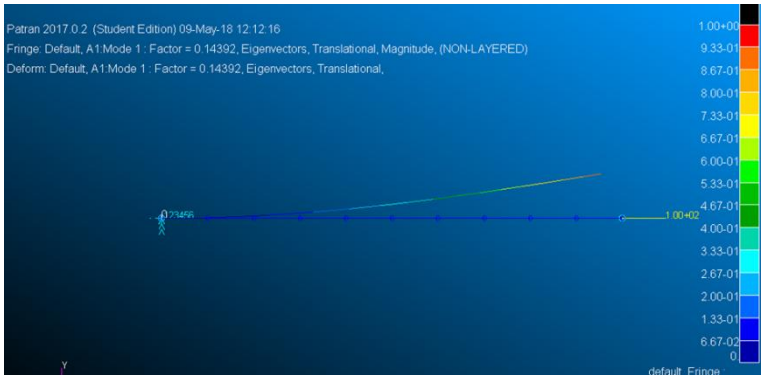

Figure 5(d): Buckling of column when one is fixed, and another is free (Case 1)

Figure 5 depicts the buckling of column for different boundary conditions for case 1 (b=d= 10 mm and L = 1000 mm). Where Figure 5(a) shows buckling of column when both ends are hinged, Figure 5(b) shows buckling of Column when both ends are fixed, Figure 5(c) shows buckling of Column when one end is fixed another is hinged and Figure 5(d) shows buckling of column when one is fixed, and another is free. From Table 2 and Fig 5(a) it's observed that the theoretical (0.5756) and analyzed buckling factor (0.5756) exactly matching with 0.0 % error with 100 % accuracy. Similar observations can be made in Fig 5(d) with theoretical (0.1439) and analyzed buckling factor (0.1439) 0.0 % error. From Fig 5(b) it's observed that there is a slight error of 0.0608% in theoretical (2.3024) and analyzed buckling factor (2.301) with 99.93 % accuracy followed by Fig 5(c) with theoretical (1.1512) and analyzed buckling factor (1.1772) 2.2585 % error with 97.74 % accuracy. Similar observations were noted by Li et al. [19].

3.2 BUCKLING FACTOR CALCULATIONS OF CASE 2 (b= 20 mm, d= 10 mm, and L = 1000 mm)

By considering the rectangular cross section at applied load i.e., width of 20mm, thickness of 10mm and the length of panel 1000 mm the calculations are done. We got the results as in the table below. Here the low moment of inertia for the theoretical calculations is considered because the panel will buckle at that region.

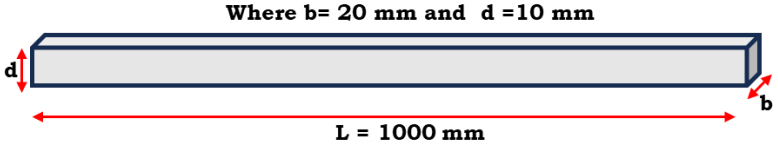

Figure 6: Rectangular shape of b= 20 mm, d= 10 mm, and L= 1000 mm

The calculations are done based on the effective length dimension for different boundary conditions (Case A, B, C and D) as displayed in Figure 2, 6 and Eqn (i).

Table 3: Calculated values of different boundary conditions

S/No	Case	P_{cr}	E	I	L_e Conditions	BF
1	A	115.145	$70 *10^3$	1666.67	$L_e = L$	1.15145
2	B	460.582			$L_e = 0.5L$	4.60582
3	C	230.295			$L_e = 0.7L$	2.30295
4	D	28.786			$L_e = 2L$	0.28786

Case A Calculations

$I = \frac{d*b^3}{12} = \frac{20*10^3}{12} = 1666.67; P_{cr} = \frac{\pi^2*7000*1666.67}{(1000)^2} = 115.145$; BF = 115.145/ 100 = 1.15145

Case B Calculations

$P_{cr} = \frac{\pi^2*7000*1666.67}{(1000/2)^2} = 460.582$;BF = 460.582/ 100 = 4.60582

Case C Calculations

$P_{cr} = \frac{\pi^2*7000*1666.67}{(0.7071*1000)^2} = 230.295$; BF = 230.295/ 100 = 2.30295

Case D Calculations

$P_{cr} = \frac{\pi^2*7000*1666.67}{(2*1000)^2} = 28.786$; BF = 28.786/ 100 = 0.28786

3.2.1: BUCKLING FACTOR USING NASTRAN-PATRAN ANALYSIS OF CASE 2

Theoretical buckling factor is calculated as explained above for different boundary conditions as explained in section 3.2.

Table 4: Theoretical and Analyzed values of case 2 for buckling factor at different boundary conditions

S/No	Case	L_e Conditions	BF (Theoretical)	BF (Analyzed)	%Error	Accuracy
1	A	$L_e = L$	1.15145	1.1512	0.0002	99.99998
2	B	$L_e = 0.5L$	4.60582	4.6021	0.0825	99.9962
3	C	$L_e = 0.7L$	2.30295	2.3543	0.0511	99.9489
4	D	$L_e = 2L$	0.28786	0.2878	0.0000	100.00000

Case A: NASTRAN-PATRAN Analysis

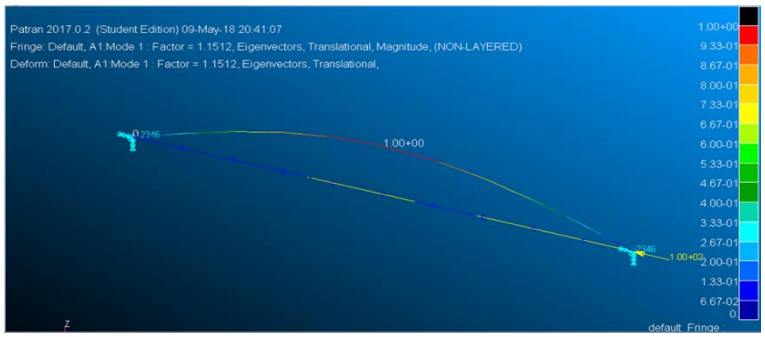

Figure 7(a): Buckling of column when both ends are hinged (Case 2).

Case B: NASTRAN-PATRAN Analysis

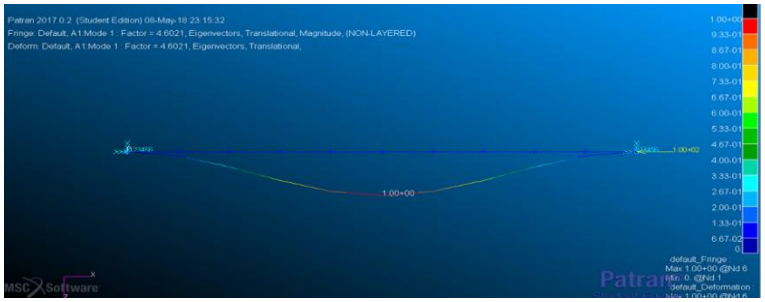

Figure 7(b): Buckling of Column when both ends are fixed (Case 2).

Case C: NASTRAN-PATRAN Analysis

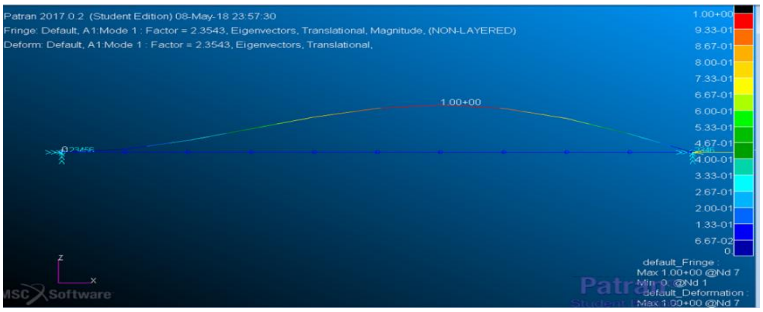

Figure 7(c): Buckling of Column when one end is fixed another is hinged (Case 2).

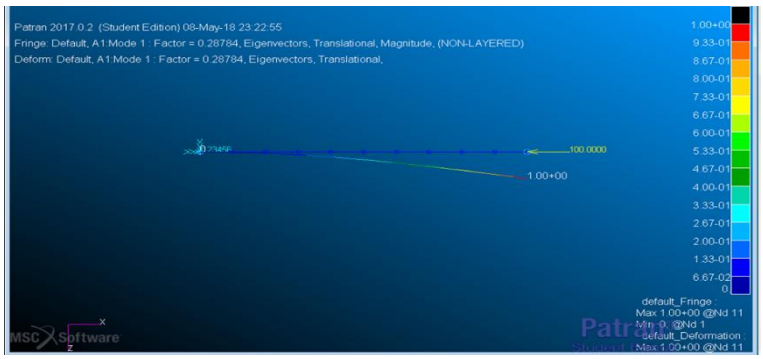

Figure 7(d): Buckling of column when one is fixed, and another is free (Case 2).

Figure 7 depicts the buckling of column for different boundary conditions for case 2 (b= 20 mm, d= 10 mm, and L = 1000 mm). Where Figure 7(a) shows buckling of column when both ends are hinged, Figure 7(b) shows buckling of Column when both ends are fixed, Figure 7(c) shows buckling of Column when one end is fixed another is hinged and Figure 7(d) shows buckling of column when one is fixed, and another is free. From Table 4 and Fig 7(a) it's observed that the theoretical (1.15145) and analyzed buckling factor (1.1512) with a slight error of 0.0002 % with 99.99 % accuracy. From Fig 7(d) it can be observed that theoretical (0.2878) and analyzed buckling factor (0.2878) are same 0.0 % error and 100 % accuracy. From Fig 7(b) it's observed that there is a slight error of 0.0825 % in theoretical (4.6058) and analyzed buckling factor (4.6021) with 99.93 % accuracy followed by Fig 7(c) with theoretical (2.3029) and analyzed buckling factor (2.3543) 0.0511 % error with 99.94 % accuracy. Similar observations were noted by Coşkun et al. [20]

4. Conclusion

The present study used the finite element analysis method to thoroughly investigate and analyse the one-dimensional column buckling factor of the Al2024 alloy panel structure. From the studies, it was concluded that:

(i) The buckling factors were effectively determined for various boundary conditions by considering the panel's dimensions, including length, width, and thickness.

(ii) Theoretical and analyzed buckling factors calculated using Nastran-Patran for the Panel were in line with each other.

(iii) The highest critical load (Pcr) and buckling factor of case 1 (b=d= 10 mm and L = 1000 mm) were found for the column when both ends are fixed, followed by the column with one end fixed another is hinged, column when both ends are hinged, and column when one is fixed, and another is free.

(iv) The highest critical load (Pcr) and buckling factor of case 2 (b= 20 mm, d= 10 mm, and L = 1000 mm) were alike that of case 1, i.e., the column when both ends are fixed, followed by the column with one end fixed another is hinged, column when both ends are hinged, and column when one is fixed, and another is free.

(v) Overall, it can be analyzed that loaded edges with fixed boundary conditions will give a better buckling factor for both case 1 and 2.

References

[1] Lakshmikanthan Avinash.; Angadi, S.; Malik, V.; Saxena, K.K.; Prakash, C.; Dixit, S.; Mohammed, K.A. (2022) "Mechanical and Tribological Properties of Aluminum-Based Metal-Matrix Composites". Materials 2022, 15, 6111. https://doi.org/ 10.3390/ma15176111.

[2] Vedernikov A, Safonov A, Tucci F, et al. Pultruded materials, and structures: A review. J Compos Mater 2020; 54(26):4081–4117.10.1177/0021998320922894.

[3] Zhang DD, Zhao QL, Huang YX, et al. Flexural properties of a lightweight hybrid FRP-aluminum modular space truss bridge system. Compos Struct 2014; 108:600–615.10.1016/j.compstruct.2013.09.058

[4] Li F, Deng AZ, Zhao QL, et al. Research on Influence mechanism of composite interlaminar shear strength under normal stress. Sci Eng Compos Mater 2020; 27:119–128.10.1515/secm-2020-0011 Pp570-580. https://doi.org/10.1016/j.jallcom.2019.01.382.

[5] Zhang DD, Lv YR, Zhao QL, et al. Development of lightweight emergency bridge using GFRP–metal composite plate-truss girder. Eng Struct 2019; 196:109291.10.1016/j.engstruct.2019.109291

[6] Avinash Lakshmikanthan, Srikanth Bontha, M Krishna, Praveennath G Koppad, T Ramprabhu (2019) "Microstructure, mechanical and wear properties of the A357 composites reinforced with dual sized SiC particles" Journal of Alloys and Compounds-Elsevier,786(25)

[7] Chithirai Pon Selvan, L. Girisha, Vishwanath Koti, Mahadev Madgule, Mahesh B Davanageri, Avinash Lakshmikanthan, Manjunath Patel GC, (2023) Optimization of stir casting and drilling process parameters of hybrid composites, Journal of Alloys, and Metallurgical Systems, 3(100023) ISSN 2949-9178, https://doi.org/10.1016/j.jalmes.2023.100023.

[8] Manjunath Naik H R, Manjunath L H, Vinayak R. Malik, Manjunath Patel GC, Kuldeep K. Saxena & Avinash Lakshmikanthan (2021) "Effect of Microstructure, Mechanical and Wear on Al-CNTs/Graphene Hybrid MMCs". Advances in Materials and Processing Technologies, Taylor & Francis, DOI: 10.1080/2374068X.2021.1927646

[9] Vinayaka N, Avinash Lakshmikanthan, Manjunath Patel GC, Chithirai Pon Selvan, Vikram Kumar S Jain, S. A. Srinivasan & Harsha hm (2021) "Mechanical, Microstructure and Wear properties of Al 6113 Fly Ash reinforced Composites: Comparison of as cast and Heat-treated Conditions". Advances-in Materials-and-Processing-Technologies, -Taylor-&-Francis, DOI: 10.1080/2374068X.2021.1927649

[10] Praveena Bindiganavile Anand, Avinash Lakshmikanthan, Manjunath Patel GowdruChandrashekarappa, Chithirai Pon Selvan, Danil Yurievich Pimenov and Khaled Giasin (2022)" Experimental Investigation of Effect of Fiber Length on Mechanical, Wear, and Morphological Behavior of Silane-Treated Pineapple Leaf Fiber Reinforced Polymer Composites" Fibers (MDPI) 2022, 10, 56. https://doi.org/ 10.3390/fib10070056, Pp1-16.

[11] Praveena B A, Balachandra P Shetty, Vinayaka N, Srikanth H V, Shiv Pratap Singh Yadav & Avinash L (2020) "Mechanical properties and water absorption behaviour of pineapple leaf fibre reinforced polymer composites″ Advances-in-Materials-and-Processing-Technologies, -Taylor-&-Francis, DOI: 10.1080/2374068X.2020.1860354

[12] Praveena B A, Balachandra P Shetty, Sachin B, Shiv Pratap Singh Yadav & Avinash L (2020) " Physical and mechanical properties, morphological behaviour of pineapple leaf fibre reinforced polyester resin-composites″, -Advances-in-Materials-and-Processing-Technologies, -Taylor-& Francis, DOI: 10.1080/2374068X.2020.1853498

[13] Ravi YV, Avinash Lakshmikanthan, Natesan Kapilan, Manjunath Patel GC, Oguzhan Der, Ali Ercetin (2023) "Physico-Mechanical Property Evaluation and Morphology Study of Moisture Treated Hemp-Banana Natural Fiber Reinforced Green Composites" Journal of Composites Science ,7, 266. https:// doi.org/10.3390/jcs7070266.

[14] Botelho EC, Silva RA, Pardini LC, et al. A review on the development and properties of continuous fiber/epoxy/aluminum hybrid composites for aircraft structures. Mater Res 2006; 9:247–256.10.1590/S1516-14392006000300002

[15] Sinmazçelik T, Avcu E, Bora MO, et al. 2011. A review: fibre metal laminates, background, bonding types and applied test methods. Mater Des 2011; 32: 3671–3685.10.1016/j.matdes.2011.03.011

[16] Lin Y, Huang YX, Huang T, et al. Open-hole tensile behavior and failure prediction of carbon fibre reinforced aluminium laminates. Polymer compos 2018; 39:4123–4138.10.1002/pc.24477

[17] Montesano J, Fawaz Z, Bougherara H. Use of infrared thermography to investigate the fatigue behavior of a carbon fiber reinforced polymer composite. Compos Struct 2013; 97:76–83.10.1016/j.compstruct.2012.09.046

[18] Gun T. A new functional for buckling analysis of straight bars and its finite element solution. MSc Thesis. Istanbul Technical University, Istanbul, Turkey (in Turkish), 2002

[19] Li XF, Xi LY, Huang Y (2011) Stability analysis of composite columns and parameter optimization against buckling. Composites: Part B 42: 1337-1345.

[20] Coşkun SB (2010) Analysis of tilt-buckling of Euler columns with varying flexural stiffness using homotopy perturbation method. Mathematical Modelling and Analysis 15(3):1648-3510.http://dx.doi.org/10.3846/1392-6292.2010.15.275-286